POAC'25
St. John's, Newfoundland and Labrador, Canada

Proceedings of the 28th International Conference on Port and Ocean Engineering under Arctic Conditions
Jul 13-17, 2025
St. John's, Newfoundland and Labrador
Canada

Evaluation of Monopile Wind Turbine Platforms for Extreme Design Conditions

Paul Stuckey[1], Ahmed Derradji-Aouat[2], Mark Fuglem[1], Ian Turnbull[1]
[1] C-CORE, St. John's, Canada
[2] National Research Council of Canada, St. John's, Canada

ABSTRACT

There are currently no offshore wind developments in Atlantic Canada, and there is limited experience in designing such structures for ice loads. This study highlights key design considerations for offshore wind turbines off Newfoundland's west coast, emphasizing gaps in environmental data, particularly regarding sea ice conditions and ice load models. The analysis involves application of IEC 61400-3-1 design load cases for the parked mode of a 15 MW reference turbine on a 10 m diameter monopile in 45 m water depth using OpenFAST. The region is subject to winter storms and occasional hurricanes, with design cases covering 1-, 50-, and 500-year return periods. While wind and wave loads are well characterized, uncertainties remain in ice load estimation due to limited data on ice thickness and movement. Stochastic ice loads for assumed ice thicknesses of 0.5 m and 1.0 m are included to illustrate potential ice-structure interaction effects under parked conditions.

KEY WORDS: Offshore wind turbine, parked load scenario, pack ice, monopile, OpenFAST

INTRODUCTION

Offshore wind energy has become a critical component in the global transition to renewable energy and electrification of carbon intensive power generation, with significant developments in Europe and North America. These projects commonly face complex environmental challenges, including the combined effects of wind, waves, and in some regions, ice. While offshore wind farms have been deployed successfully in various temperate and tropical locations, cold-climate environments such as Atlantic Canada pose unique design challenges due to the presence of sea ice and harsh storm conditions.

Atlantic Canada offers strong offshore wind resources with significant energy potential, particularly off coast of Newfoundland. King et al. (2025) also describe a large area off the southeast coast of Newfoundland with potential power generation on the order of 100 GW. Considerations for investors include proximity to shore, port infrastructure, grid access, market stability, and energy storage and conversion options.

Designing offshore wind turbines for Atlantic Canada requires comprehensive evaluation of extreme aerodynamic, hydrodynamic, and ice-induced loads, particularly under parked-mode conditions when turbines are idling or shut down during severe weather. While wind and wave

effects are relatively well studied, the presence of sea ice introduces additional uncertainties due to limited environmental data and modeling challenges related to ice-structure interaction.

This paper presents detailed numerical simulations of environmental loads on a 15 MW monopile-supported offshore wind turbine operating in parked mode under subjected to ice, wind, wave, and current loads. Building on a prior regional assessment of 17 potential offshore wind sites in Atlantic Canada (Fuglem et al., 2024), this study focuses on a single site located 10 to 15 km offshore from the Port-au-Port Peninsula, on the west coast of Newfoundland. With a water depth of approximately 45 m, this location is well suited monopile foundations. The site has favorable wind conditions throughout the year for energy production and has mean annual significant wave heights of less than 2 m, supporting maintenance activities. The area experiences sea ice incursions during some years, adding complexity to design and operations

The simulations utilize OpenFAST—a widely used, open-source aero-hydro-servo-elastic simulation tool—to capture coupled turbine and environmental interactions. Several IEC 61400-3-1 design load cases (DLCs) specific to the parked operational state were selected to examine the turbine's structural response to extreme loads. This approach enables a comprehensive assessment of how environmental factors differ in impact between ice and non-ice seasons and the combined loading effects on critical turbine components including the tower, substructure, and nacelle.

The results emphasize important design considerations unique to Atlantic Canada and identify significant gaps in environmental data especially related to sea ice thickness and dynamics. These findings support the development of more robust design and operational strategies to harness offshore wind energy safely and efficiently in cold-climate regions.

RELEVANT STANDARDS

The International Electrotechnical Commission (IEC) and DNV provide the primary international standards for offshore wind turbine design. These standards outline design requirements for offshore-specific conditions, including extreme wind, wave, current, and ice loading, along with the turbine's control system and structural dynamics. They define design situations such as power production, shutdowns, and parked conditions, each paired with specific Design Load Cases (DLCs) to ensure structural integrity under varying metocean and fault scenarios.

In Canada, the Canadian Standards Association (CSA) adopts and adapts IEC standards to address regional needs. The current CSA standard (CAN/CSA C61400-3) is based on the original IEC 61400-3:2009, with national deviations to reflect Canadian offshore environments. An updated version of IEC 61400-3-1 is under review for adoption, while a decision on the floating platform standard (IEC 61400-3-2) is pending. One key area of adaptation is ice loading: CSA proposes using ISO 19906:2019 instead of IEC Annex D, as it better captures the complexity of Canadian sea ice (including drifting floes, pressure ridges, and regional variability) and icebergs. The approach emphasizes calculating actual 50-year return period ice loads directly, rather than relying on assumed thickness or horizontal-only force assumptions.

Design Load Cases (DLCs) are central to both IEC and CSA-based assessments, capturing the nonlinear, dynamic nature of offshore wind turbines. These include both normal and extreme events, with partial safety factors adjusted based on load type and occurrence likelihood. Annex I of IEC 61400-3-1 has two additional DLCs based on 500-year hurricane winds, provided as a robustness check. As hurricanes can reach Canada's east coast, these may need consideration, though the hurricanes are less severe than further south.

METOCEAN AND ICE CONDITIONS

Wind, Waves and Currents

Wind speed data are available from the MSC50 database, which was developed by Oceanweather Inc. for the Meteorological Service of Canada (MSC), a division of Environment and Climate Change Canada (ECCC) (Swail et al., 2006). The MSC50 is a detailed hindcast dataset that provides wind and wave information for offshore Canadian waters. For the selected site, wind speed is reported as a one-hour average of effective neutral wind, measured in meters per second (m/s) at a height of 10 meters above mean sea level. For this study, the MSC50 database included the years 1954 to 2021. The 1-year and 50-year extreme wind speeds (1-hour averaging, 10 m height) were determined to be 22.4 m/s and 26.2 m/s, respectively.

IEC 61400-1:2019 defines the reference wind speed as the 10-minute mean wind speed with a recurrence period of 50 years at hub height. Two conversions are applied. First, the method outlined in ISO 19901-1 (Section A.7.3 *Wind profile and time-averaged wind speed*) was used to determine wind speeds at hub height given wind speeds at the 10 m reference height. Second, the conversion from 1-hour to 10-minute wind speeds was performed using the commonly used expression

$$V_{10min} = V_{1hour}\left(\frac{60}{10}\right)^{\alpha} \qquad \text{Eqn. 1}$$

where α is assumed to be 0.11. The final 1-year and 50-year extreme wind speeds (10-minute averaging, 150 m height) are 36.2 m/s and 43.0 m/s, respectively.

Wave data are also available from the MSC50 hindcast database. The 1-year and 50-year significant wave heights are 6.7 m and 9.1 m, respectively, and the associated peak periods are 10.3 and 12.3 s, respectively.

Ocean currents data are extracted from the Global Ocean Physics Analysis and the Hybrid Coordinate Ocean Model (HYCOM). The HYCOM database covers a temporal range of 22 years from January 1994 to December 2015. The temporal resolution of the output is three hours. The 1-year and 50-year significant wave heights were determined to be 0.37 m/s and 0.67 m/s, respectively.

IEC 61400-3-1 states that for offshore wind turbines installed in areas affected by tropical cyclones, additional design considerations may be needed to maintain the same safety level as for offshore wind turbines installed in extra-tropical regions. An initial analysis of hurricanes passing through the region, including western Newfoundland, the Gulf of St. Lawrence, and the south coast of Newfoundland is conducted. A total of 32 hurricanes were identified as entering the region during the period 1954-2021, corresponding to an annual rate of 0.42 yr^{-1}. In this study, the MSC50 data are divided into two categories: hurricanes and winter storms (all other data). Hurricane data are defined as all data occurring in a given month/year for which a hurricane entered the circular zone. Based on this approach, the 500-year wind speed for hurricane analysis was estimated to be 55 m/s. It should be noted that the majority of the hurricanes identified in the analysis passed through the southern part of the circular zone, several hundred nautical miles from the selected site for this study. It is likely that some of the selected hurricanes did not reach the study site at all or did so as a weakened post-tropical storm. It is of note that, given the speed at which hurricanes pass through the region, there is less time for larger waves to develop. The results are summarized in Table 1.

Table 1. Comparison of extreme wind and wave values for winter storms vs. hurricanes

Parameter	Return Period	Winter Storms	Hurricanes
Wind speed (m/s); 10-min avg, hub height	1	36.2	
	50	43.0	
	500		55.0
Hs (m)	1	6.7	
	50	9.1	
	500		10.7
Tp (s)	1	10.3	
	50	12.3	
	500		12.0
Current speed (m/s)	1	0.37	
	50	0.67	
	500		0.67*

* assumed 50-year current

Sea Ice

Sea ice conditions in the Gulf of St. Lawrence can be complex and varied. The ice is generally thicker in the north and can include small amounts of old ice and even icebergs that pass through the Strait of Belle Isle. Though old ice and icebergs could potentially reach Site 3, the probability is quite small. As one moves south in the gulf, the ice season is generally shorter and the ice thinner, though ice can preferentially grow around Prince Edward Island and further east along Quebec's north shore and at the mouth of the St. Lawrence River. Strong, persistent winds can carry thicker ice to Site 3 in some years. The amount of ice in the Gulf also varies significantly from year to year, with nearly full coverage in extreme years.

Kubat et al. (2010) provide a good overview of the variables in ice conditions and the challenges in modelling sea ice conditions in the Gulf. Classifying ice chart zones based on partial concentrations of ice of given sizes and thicknesses of floes, and modelling changes and movements of these zones, as well as the formation of ridges, can be very challenging. While the Canadian Ice Service (CIS) provides invaluable data in the form of ice charts, more detailed environmental surveys and modelling of the movement and fate of sea ice under different wind conditions are critical for understanding and predicting sea ice loads on offshore wind turbines. Their study focused on modelling ice conditions in the southern part of the Gulf and on the region west of Prince Edward Island, where a shear zone and heavy ridging close to shore in shallower water occurred. Modelling such movements and rubbling of ice will be especially important in understanding the interaction of sea ice with the multiple structures in a wind farm.

Fuglem et al. (2024) estimated the amount of ice crushing as a function of ice thickness for Site 3 based on CIS ice charts. While the charts indicate that there could be limited crushing associated with ice thickness up to 1.6 m, there is some concern that the ice charts err on the conservative side. In this paper, a 1-year thickness of 0.5 m and a 50-year thickness of 1.0 m are suggested for illustration. IEC 61400-3-1 provides a model for level ice growth given the number of freezing degree days that could also be considered.

EXAMPLE DESIGN CHECKS AND DISCUSSION

OpenFAST is used to evaluate design load cases for the 'parked design' situation for a 15 MW offshore wind turbine supported by a monopile foundation. This study focuses on identifying key design drivers under extreme environmental conditions and understanding the strengths,

limitations, and assumptions within the modeling approach, particularly regarding the representation of ice loads.

The analysis is performed using OpenFAST v3.5, an open-source, coupled aero-hydro-servo-elastic simulation tool developed and maintained by the U.S. National Renewable Energy Laboratory (NREL). To simulate atmospheric turbulence, wind fields were generated using TurbSim, NREL's stochastic wind field simulator (Jonkman, 2009). Together, these tools provide a comprehensive framework for evaluating the dynamic response of offshore wind turbines subjected to complex environmental conditions, including wind, wave, and ice interactions.

The wind turbine model is based on the IEA Wind TCP 15 MW reference wind turbine, a Class IB according to IEC 61400-3-1 (see Figure 1). The turbine has a rotor diameter of 240 meters, a hub height of 150 meters, and is mounted to a 10-meter diameter monopile in 45 meters of water depth, representative of Site 3. This monopile configuration provides a practical and widely adopted fixed-bottom support structure for shallow to moderate-depth offshore wind sites. Additional technical specifications and model details are available in the IEA Wind TCP Task 37 report (Gaertner et al., 2020).

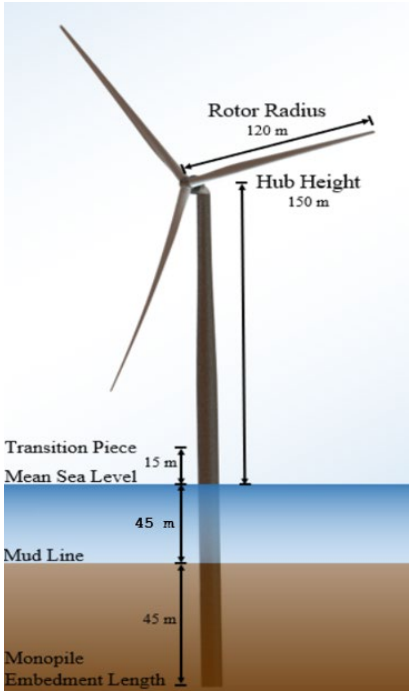

Figure 1. IEA Wind TCP 15 MW reference wind turbine; from Gaertner et al. (2020)

Analysis of Cases for the Parked Design Scenario without Sea Ice

The ultimate limit state (ULS) normal cases for the parked design scenario are selected for this study to investigate structural loading on an offshore wind turbine under extreme environmental conditions, without ice present. DLC 6.1 requires the combination of wind and wave conditions such that the joint environmental loading corresponds to a 50-year return period. In the absence of a detailed analysis of site-specific directional data, a wind-wave misalignment within ±30° is assumed. For turbines with active yaw systems, a mean yaw misalignment of ±8° is imposed.

DLC 6.2 represents a scenario in which the wind turbine experiences a loss of electrical power

supply at an early stage of a storm containing an extreme wind event. In this condition, unless a backup power system is available to maintain yaw control and blade pitch regulation for a minimum of six hours, the analysis must account for a potential wind direction shift of up to ±180. The adoption of robust backup systems, including battery-supported yaw and pitch control, has largely mitigated the conditions that DLC 6.2 is intended to address; this case was not considered for this paper.

DLC 6.3 considers the combination of a 1-year return period extreme wind event with an extreme yaw misalignment scenario. A yaw offset of up to ±20° was imposed. The simulation methodology for DLC 6.3 followed the same conventions as DLC 6.1, allowing for consistent application of extreme wind and wave inputs during turbine operation with control active.

The design of offshore wind turbines in cyclone-prone regions requires special attention. For such environments, IEC 61400-1 and IEC 61400-3-1 provide additional guidance for a robustness check considering wind speeds and wave heights with 500-year return periods and incorporating cyclone-specific characteristics such as increased vertical wind shear, significant wind veer, and realistic wind-wave pairing via joint probability or response-based methods.

For this study, 16 non-ice cases (see Table 2) are defined covering a range of wind speeds (1-, 50- and 500-year return periods), yaw and wind-wave misalignments, and parked mode (idling or standstill) to capture extreme load scenarios.

Table 2. Summary of non-ice cases

Non-Ice Case	Rotor	Wind Speed (m/s)	Significant Wave Height (m)	Yaw Misalignment (°)	Wind-Wave Misalignment (°)
1	Idle	43.0	9.1	0	0
2				8	15
3				8	30
4	Standstill				
5					
6					
7	Idle	36.2	6.7	0	0
8				10	10
9				20	30
10	Idle	55.0	10.7	0	0
11				5	10
12				20	30
13	Standstill			0	0
14				5	10
15				20	30
16	Production	10	2.4	0	0

One 10-minute simulation was performed for each load case. While the IEC 61400 standards recommend multiple simulations, such as a minimum of six 1-hour simulations or six sets of six 10-minute simulations, to ensure statistical reliability, the purpose here is to compare the structural response for the different DLCs.

The ninety-percentile values for the input wind speed and a select set of response parameters are shown in Table 3 and Table 4. These parameters were selected to highlight critical structural and dynamic responses of the offshore wind turbine system. Tower-related quantities such as

nacelle acceleration, top displacement, base force, and bending moments reflect the turbine's global motion and load transfer under aerodynamic and hydrodynamic loading. Monopile parameters such as the hydrodynamic force, mudline shear and moment, surge, and pitch provide insight into the behavior of the monopile.

Table 3. Ninety-percentile structural responses for design load cases without sea ice (1 of 2)

Case	Wind x vel.	Nacelle x acc.	Nacelle y acc.	Surge at WL	Pitch at WL	Tower top x disp.	Tower top y disp.	Thrust (MN)
	m/s	m/s^2	m/s^2	m	deg	m	m	
1	40.3	0.55	0.27	0.054	0.089	0.22	-0.24	414
2		0.55	0.27	0.061	0.103	0.30	0.21	481
3		0.49	0.29	0.054	0.089	0.23	0.25	460
4		0.49	0.30	0.045	0.073	0.12	-0.55	376
5		0.50	0.29	0.056	0.094	0.26	0.14	464
6		0.43	0.30	0.048	0.081	0.19	0.15	444
7	36.2	0.61	0.27	0.052	0.089	0.23	-0.07	432
8		0.60	0.22	0.054	0.092	0.26	0.27	479
9		0.51	0.34	0.033	0.055	0.07	0.89	339
10	55.0	0.60	0.40	0.081	0.137	0.46	-0.40	417
11		0.55	0.40	0.084	0.145	0.51	-0.01	491
12		0.63	0.59	0.070	0.118	0.39	1.84	268
13		0.53	0.42	0.067	0.111	0.30	-0.97	374
14		0.52	0.36	0.082	0.137	0.45	-0.34	494
15		0.46	0.52	0.047	0.078	0.15	1.64	228
16	10.0	0.20	0.25	0.145	0.265	1.22	-0.10	2,297

Table 4. Ninety-percentile structural responses for design load cases without sea ice (2 of 2)

Case	Hydrodyn. x force	Blade tip x disp.	Mudline x shear	Mudline y moment	Tower base x force	Tower base y moment
	MN	m	MN	MN-m	MN	MN-m
1	3.76	6.11	4.39	172	1.23	60
2	3.49	2.47	4.09	179	1.32	72
3	2.97	2.47	3.59	156	1.23	61
4	3.78	9.90	4.31	153	1.13	42
5	3.51	4.12	4.11	170	1.24	64
6	3.00	4.12	3.60	148	1.15	52
7	2.85	3.76	3.32	146	1.18	59
8	2.69	1.56	3.23	151	1.21	64
9	1.81	0.95	2.25	99	0.95	33
10	4.51	9.85	5.37	241	1.64	100
11	4.32	6.30	5.23	251	1.65	106
12	3.70	-0.56	4.40	202	1.50	87
13	4.55	16.06	5.40	209	1.49	74
14	4.43	10.30	5.34	245	1.62	97
15	2.93	-6.00	3.64	143	1.26	47
16	1.24	13.34	3.05	361	2.17	226

Cases 1–3 examine the effects of yaw and wind-wave misalignment. As yaw and wind-wave misalignment increase, tower top displacements (especially in the y-direction) rise noticeably, indicating greater lateral motion and potential structural sensitivity. Thrust and hydrodynamic forces show moderate variation, with a slight reduction in Case 3, suggesting that certain misalignment angles may reduce overall aerodynamic loading. Blade tip deflections and

mudline shear forces decrease across the three cases, possibly due to reduced effective wind loading on the blades. Tower base and mudline moments vary slightly but remain within a similar range, showing some redistribution of loads. Overall, yaw misalignment has a more noticeable impact than wind-wave misalignment, influencing structural dynamics by altering load paths and reducing certain peak responses, while increasing lateral motions that could affect fatigue and serviceability.

Cases 16, 7, 1, and 10 illustrate how the turbine responds to increasing wind speed, from 10 m/s in Case 16 to 55 m/s in Case 10. As wind speed rises, thrust and hydrodynamic forces generally increase, leading to higher mudline shear and tower base forces. However, some displacements and accelerations (e.g., nacelle acceleration and tower top motion) do not scale linearly, indicating complex interactions between aerodynamic damping, structural stiffness, and load redistribution. Case 16 (lowest wind speed) shows the highest tower top displacement and pitch, likely due to reduced aerodynamic damping during standstill. In contrast, Case 10 shows significantly higher blade tip deflections and mudline moments, highlighting the structural demand during extreme wind events. These trends emphasize the importance of accounting for both low- and high-wind parked conditions in design to capture the full range of turbine responses.

A comparison between idling and standstill conditions at both moderate (Cases 1 and 4) and extreme wind speeds (Cases 10 and 13) reveals consistent trends in turbine response due to the loss of aerodynamic damping. At a 50-year return wind speed, the standstill case (Case 4) exhibits a slightly lower thrust load, nacelle acceleration, and hydrodynamic forces compared to the idling case (Case 1). However, tower top y-displacement is more than double in Case 4, and blade tip displacement also increases significantly, indicating greater structural motion. A similar and slightly more pronounced pattern is observed in the extreme wind speed cases. In Case 13 (standstill), thrust drops from 417 MN (Case 10, idling) to 374 MN, while tower top y-displacement increases to −0.97 m (from −0.40 m), and blade tip deflection rises to 16.06 m (from 9.85 m). These results highlight how standstill conditions reduce aerodynamic loading but allow for larger structural excursions due to reduced damping.

Analysis of Cases for the Parked Design Situation with Sea Ice

There are three design load cases for sea ice for the parked design situation at Site 3, namely: D6, ultimate loads given pressure from hummocked ice and ice ridges; D7, fatigue loads given horizontal load from moving ice at relevant velocities; and D8, ultimate loads given horizontal load from moving ice at relevant velocities.

The design load case D6 includes loads from ridges and rubble. For ridge interactions with vertical cylindrical structures, the load may be modelled as the sum of a crushing load associated with the consolidated layer of the ridge and either local passive or global plug failure of the unconsolidated part of the ridge (Palmer & Croasdale, 2013; Samardžija et al., 2025). The load associated with the unconsolidated part of the ridge is generally much smaller than that associated with the consolidated layer. The consolidated layer is generally thicker than the surrounding level ice, but weaker, and there is uncertainty regarding the extent to which ice ridges could create greater loads. If grounded rubble in shallower water builds up against the turbine structures, it could potentially impart a significant load. The presence of arrays of fixed monopile structures could influence this rubbling, even though the towers are generally quite far apart.

The design load case D7 considers the contribution of vibration during the parked design scenario to fatigue. It is of note that the 25 m/s cut-out speed of the platform during the heavier

part of the sea ice season occurs around 0.3 percent of the time. The contribution to fatigue will only be significant if ice-induced vibration is more significant during periods with higher wind. If the ice moves faster with the higher wind speeds, then crushing is more likely in preference to ice-induced vibration. Detailed environmental surveys and modelling would be required to determine the exposure to ice movements with lower velocities that could induce larger vibrations.

The design load case D8 considers interactions with level ice. Failure modes could include creep, intermittent crushing, frequency lock-in and random crushing depending on the ice velocity. The reader is referred to Hendrikse (2017) and Hendrikse et al. (2018) for recent work on the different failure modes. In this paper, only random crushing is considered. The design load case indicates that load traces associated with the 50-year ice thickness should be considered. In contrast, ISO 19906:2019 indicates that both a 50-year ice thickness in combination with a 1-year ice strength and a 1-year ice thickness in combination with a 50-year ice strength should be considered.

For random crushing, Kärnä's stochastic crushing model, as implemented with the IceFloe package with OpenFAST, has been applied. Random crushing occurs at higher ice velocities, which could be more likely during the strong wind conditions associated with parked turbine conditions, though the extent to which this occurs needs validation. Kärnä et al. (2007) provide observations of failure modes based on long-term visual observations for the Norströmsgrund lighthouse. They note that when the ice was thicker than 0.20 m and the diameter of sheet ice was at least 50 times the structure diameter, more than 60% of loading events resulted in random crushing. For ice thinner than 0.3 m, flexural and mixed failure modes were common. Small floes usually failed by splitting (these were likely under significant pressure, otherwise, they would have moved around the structure). They note that dynamic and creep-buckling sometimes occurred and that different failure modes were observed for ridge interactions.

Kärnä et al. (2007) present a model that can be used for simulating random load time series for the case of crushing of level ice during interactions with vertical structures. The model is calibrated based on observed data from the Norströmsgrund lighthouse in the Northern Baltic Sea and a mooring pole in the Bohai Sea. Interactions where a random crushing failure mode occurred and was stationary over the duration of the given events (in the order of around 100 m of crushing) were selected for analysis; i.e., the mean and variance of the random ice load over small areas remain approximately constant for these events.

Empirical auto- and cross-spectral density functions for the local forces were determined so that the variation of the pressures in space and time over the contact interface could be modelled. The implementation in IceFloe does not consider the cross-correlation, instead, it scales the loads based on a form of Eqn. 2 to account for the given reference strength, ice thickness and structure width.

Ten design load cases (Table 5) are provided to illustrate the differences between production versus parking, idling versus standstill and different ice thicknesses and directions of ice movement to the wind direction. The cases are all for level ice interactions; only the random crushing failure mode is considered in this paper. The cases were selected to illustrate how the reference ice strength should be determined and to show the influence of the different assumptions on key structural responses. The method for determining the reference strengths used in the random crushing model is described below.

Table 5. Design load cases with sea ice

Case	Rotor	Wind Speed (m/s)	Sea ice				
			Thickness (m)	Direction wrt wind (deg.)	C_R (MPa)	F_D (MN)	Reference strength (MPa)
1	Idling	36.2	0.5	0	1.02	4.71	1.1
2				90			
3			1	0	0.64		0.73
4				90			
5	Standstill	36.2	1	0	0.64	4.71	0.73
6				90			
7	Production	10	0.5	0	1.66	6.79	1.78
8				90			
9			1	0	1.27	9.34	1.46
10				90			

The IEC 61400-3-1 design load case D8 requires that a 50-year ice thickness be considered. IEC 61400-3-1 Eqn. D.5 gives the maximum static force H_d on a vertical cylindrical structure

$$H_d = C_R \left(\frac{h}{h_1}\right)^n \left(\frac{D}{h}\right)^m \times A_C \qquad \text{Eqn. 2}$$

where A_C is the contact area (equal to the structure diameter D times ice thickness h), C_R is an ice strength coefficient, h_1 is a reference ice thickness of 1 m, m equals -0.16 and n equals $-0.5 + h/5$ for h < 1 m and -0.3 for $h \geq 1$m. C_R varies depending on the location, ranging from 1.8 in subarctic regions such as the Baltic Sea and Grand Banks, to 2.8 for Arctic conditions. Reference is also made to the 2010 version of ISO 19906. In ISO 19906:2019, a multiplicative correction factor f_{AR} for narrow structures is included, where $f_{AR} = e^{\frac{-D}{3h}}\sqrt{1 + 5\frac{h}{D}}$. The standard indicates that if the horizontal displacement of the structure at the waterline can exceed 10 mm, dynamic effects should be considered.

Care is required in selecting a value of C_R. Ice loads are random, and the peak load will depend on the mode of failure, the return period of interest and the amount of ice crushed each year. The value of 1.8 for the Baltic was based on ice speeds higher than 0.1 m/s and limited structural response such that the magnification effects due to structural compliance do not occur. The value of 1.8 is appropriate for 100-year loads where the exposure is similar to the ice conditions on which the value was based. Judgment and conservatism in the choice of the 1.8 value; Hendrikse and Owen (2023) provide further insight.

ISO 19906:2019 provides a mechanism to account for the exposure to ice crushing when determining C_R. The method is based on a work by Gravesen and Kärnä (2009) with enhancements by Thijssen and Fuglem (2015). Assuming a Gumbel extreme value distribution, the coefficient C_R associated with a given target annual probability of exceedance can be expressed as

$$C_R = \alpha \cdot \left(-ln\left(-ln(1 - APE)\right)\right) + \mu + \alpha + \ln(N) \qquad \text{Eqn. 3}$$

where N is α and μ depend on the location, and N depends on the exposure (distance of crushing per year). For conditions similar to the Norströmsgrund location in the Baltic, α = 0

.1092 MPa and μ = 0.7057 MPa. N is given as 220 d/135, where d is the annual length of ice crushed. This equation provides the values in Table A.8-4 of ISO 19906:2019. The annual probability of exceedance for a 1-in-50-year event is 0.02, and for a 1-year event is 0.5.

Fuglem et al. (2024) estimated approximately 75 km of ice crushing at Site 3 (see Figure 11) from CIS ice charts, based on ice floes with diameters greater than 60 m and assuming an average ice drift speed of 0.1 m/s. The wind speed exceeds 25 m/s for 0.3 percent of the time. The corresponding values of C_R for the production and parked cases, assuming a 1-year ice strength for the 50-year ice thickness and a 50-year ice strength for the 1-year ice thickness, are included in Table 5, as well as maximum static force values F_D determined using Eqn. 2. The reference strength value was determined by running the random ice strength model and varying the reference strength until the maximum force F_D is obtained for a 600-second simulation.

The resulting ninety-percentile values for select inputs and response parameters are shown in Table 6 and Table 7. The 50-year sea ice forces are smaller for the 'parked' case because the winds only exceed 25 m/s for 0.3 percent of the time, so the exposure is much less. Larger ice forces occur for the 50-year ice thickness (1 m) with a 1-year ice strength than for the 1-year ice thickness (0.5 m) with a 50-year ice strength. This shows that ice thickness is more critical than differences in ice strength, which is a function of the variance in the ice strength. The nacelle accelerations are largest for the production case when the ice moves at 90 degrees relative to the wind, when the damping on vibrations associated with random ice crushing is smallest. The tower top displacement is relatively small for the parked case, even though the 1-year wind speed is significantly greater than for the production case, the total wind resistance is smaller. In general, the responses for the random crushing cases are not as significant as those for the production mode.

Some observations from the load traces are of interest. The ice forces vary over much higher frequencies than the wind. The ice forces tend to dominate over the wind forces in the direction of wind and ice movement. The shear forces and moments due to ice loading are higher at the mudline than at the tower base, while the resulting displacement at the tower top is greater than at the water line; both of the results are to be expected.

In the direction normal to the ice and wind movement, the movement of the structure and the loads and moments at the mudline and tower base are dominated by the wind and appear to result from a lack of damping. It should be noted that the random crushing model, as implemented in OpenFAST, only simulates ice loads in the direction of ice movement. This is not realistic as crushing on a cylindrical structure should include random loads in the direction normal to the ice movement. This could have a significant effect in damping out movements in the direction perpendicular to the ice movement and should be investigated further.

The deflection of the blade tips follows a sinusoidal pattern at a period equal to the time for the blade to make a complete rotation, given the average speed during idling of around 0.2 rpm. The next steps in the analysis will be to look at how the different signals correlate, the key frequency components and any phase lags and spectral peaks.

Table 6. Ninety-percentile structural responses for design load cases with sea ice (1 of 2)

Case	Wind x vel.	Sea ice x force	Sea ice y force	Nacelle x acc.	Nacelle y acc.	Surge at WL	Pitch at WL	Tower top x disp.	Tower top y disp.
	m/s	kN	kN	m/s^2	m/s^2	m	deg	m	m
1	42.1	3.14	0	0.35	0.23	0.047	0.061	0.01	-0.11
2		0	3.14	0.16	0.40	0.001	-0.005	-0.25	0.02
3		3.53	0	0.38	0.23	0.054	0.070	0.05	-0.11
4		0	3.53	0.16	0.43	0.001	-0.005	-0.25	0.04
5		3.53	0	0.33	0.25	0.045	0.053	-0.06	-0.36
6		0	3.53	0.16	0.34	0.000	-0.008	-0.27	-0.24
7	13.0	5.08	0	0.23	0.27	0.197	0.332	1.45	-0.13
8		0	5.08	0.25	0.89	0.152	0.282	1.31	0.77
9		7.06	0	0.28	0.28	0.219	0.357	1.54	-0.12
10		0	7.06	0.32	1.23	0.158	0.291	1.35	1.16

Table 7. Ninety-percentile structural responses for design load cases with sea ice (1 of 2)

Case	Hydrodyn. x force	Blade tip x disp.	Mudline x shear	Mudline y moment	Tower base x force	Tower base y moment
	MN	m	MN	MN-m	MN	MN-m
1	1.1	3.5	4.3	176	0.8	7.8
2	0.2	3.5	0.7	14.1	0.6	-20.7
3	1.3	3.5	4.8	198	0.9	12.1
4	0.2	3.5	0.7	14.2	0.6	-20.7
5	1.2	7.2	4.8	179	0.8	-5.6
6	0.3	7.2	0.8	11.8	0.6	-24.2
7	1.0	13.5	7.3	553	2.3	236
8	0.6	13.6	2.6	372	2.3	242
9	1.4	13.5	9.4	639	2.4	240
10	0.6	13.7	2.7	387	2.4	249

CONCLUSIONS AND RECOMMENDATIONS

The findings of this study highlight some of the unique aspects of offshore wind development in Atlantic Canada, where turbines may be exposed to strong extratropical storms, weakened hurricanes, and seasonal sea ice. The analysis emphasizes the critical role of turbine operational mode and the effect on structural loading, especially under extreme wind conditions. Misalignments in yaw and wind-wave directions influence load paths and platform response, with effects more pronounced in standstill than in idling. Idling provides aerodynamic damping, which reduces extreme motions but introduces higher thrust and nacelle accelerations.

As discussed, hurricanes can reach Atlantic Canada but are often diminished in strength by the time they arrive. When performing a robustness check for such events, according to IEC 61400-1, the partial safety factor for hurricanes is 1.0, compared to 1.35 used for other normal design

situations. A comparison between 50-year extreme wind cases and 500-year hurricane cases shows increased structural demands during hurricanes, particularly in standstill scenarios. The results confirm the use of idling (free-rotor) control as an effective load mitigation strategy during high wind events. While nacelle motions and global displacements remain similar between idling and standstill, internal structural responses are considerably lower during idling.

When ice loads are included in the analysis, the random crushing of level ice during the parked design scenario does not appear to cause significant issues compared to the power production design scenario. This is largely due to the relatively small exposure (i.e., winds high enough to require parking occur only 0.3% of the time, and the probability of severe ice conditions simultaneously is reduced).

Other failure modes such as ice-induced vibration and interactions with ridges and hummock fields should be further investigated, although the exposure for these will likely also be relatively small. IEC 61400-3-1 notes that damping in the parked mode is less than in production mode, increasing the likelihood of frequency lock-in vibrations.

The next steps in the analysis will involve examining how different signals correlate, identifying key frequency components, and investigating phase lags and spectral peaks.

The most important recommendation is to initiate enhanced surveillance of wind, wave, current, and ice conditions and movements at locations in the Gulf where wind power production is feasible in the future. For ice loads, detailed measurements of ice thickness, ridges, rubbling, and ice velocity are critical. Developing improved modelling techniques to assess the potential influence of wind turbine arrays on sea ice conditions and movements is equally important, particularly for production mode. Such modelling would also be valuable for evaluating the effectiveness of proposed ice protection structures. Finally, enhanced modelling of ice-induced vibration is necessary, and recent work conducted in Europe in this area should be referenced.

REFERENCES

Fuglem, M., Stuckey, P., Derradji-Aouat, A., McKenna, R., & Ralph, F. (2024). Development of Offshore Wind in Atlantic Canada: Regulations, Standards and Technical Challenges. OCEANS 2024 - Halifax, 1–10. https://doi.org/10.1109/OCEANS55160.2024.10753762.

Gaertner, E., Rinker, J., Sethuraman, L., Zahle, F., Anderson, B., Barter, G., Abbas, N., Meng, F., Bortolotti, P., Skrzypinski, W., Scott, G., Feil, R., Bredmose, H., Dykes, K., Sheilds, M., Allen, C., & Viselli, A. (2020). Definition of the IEA 15-Megawatt Offshore Reference Wind Turbine (NREL/TP-5000-75698). Golden, CO: National Renewable Energy Laboratory. https://www.nrel.gov/docs/fy20osti/75698.pdf.

Gravesen, H., & Kärnä, T. (2009). Ice loads for offshore wind turbines in Southern Baltic Sea. Proceedings of the 20th International Conference on Port and Ocean Engineering Under Arctic Conditions, POAC9-3.

Hendrikse, H. (2017). Ice-Induced Vibrations of Vertically Sided Offshore Structures [Ph.D. Thesis]. Delft University of Technology.

Hendrikse, H., & Owen, C. (2023). Application of the suggested ice strength coefficients in ISO 19906 to intermittent crushing. Proceedings of the 27th International Conference on Port and Ocean Engineering under Arctic Conditions. 27th International Conference on Port and Ocean Engineering under Arctic Conditions, Glasgow, United Kingdom.

Hendrikse, H., Ziemer, G., & Owen, C. C. (2018). Experimental validation of a model for

prediction of dynamic ice-structure interaction. Cold Regions Science and Technology, 151, 345–358. https://doi.org/10.1016/j.coldregions.2018.04.003.

IEC 61400-3-1. (2019a). Wind energy generation systems – Part 3-1: Design requirements for fixed offshore wind.

IEC 61400-3-2. (2019). Wind energy generation systems – Part 3-2: Design requirements for floating offshore wind.

ISO 19901-1. (2015). Petroleum and natural gas industries — Specific requirements for offshore structures.

ISO 19906. (2019). Petroleum and natural gas industries - Arctic offshore structures.

Jonkman, J. (2009). TurbSim User's Guide: Version 1.50 (NREL/TP-500-46198). National Renewable Energy Laboratory. https://www.nrel.gov/docs/fy09osti/46198.pdf.

Kärnä, T., Qu, Y., Bi, X., Yue, Q., & Kuehnlein, W. (2007). A Spectral Model for Forces Due to Ice Crushing. Journal of Offshore Mechanics and Arctic Engineering, 129(2), 138–145. https://doi.org/10.1115/1.2426997.

King, T., Stuckey, P., & Fuglem, M. (2025, July). Power Generating Potential on the Grand Banks Using Fixed-Bottom Wind Turbines. 28th International Conference on Port and Ocean Engineering under Arctic Conditions (POAC'25), St. John's, Canada.

Kubat, I., Sayed, M., Savage, S. B., & Carrieres, T. (2010). Numerical simulations of ice thickness redistribution in the Gulf of St. Lawrence. Cold Regions Science and Technology, 60(1), 15–28. https://doi.org/10.1016/j.coldregions.2009.07.003.

Palmer, A., & Croasdale, K. (2013). Arctic offshore engineering. World Scientific.

Petroleum and Natural Gas Industries - Arctic Offshore Structures, Pub. L. No. 19906 (2019).

Samardžija, I., Høyland, K. V., Leira, B. J., & Naess, A. (2025). Probabilistic assessment of first-year ice ridge action on offshore structures. Cold Regions Science and Technology, 231, 104410. https://doi.org/10.1016/j.coldregions.2024.104410.

Swail, V., Cardone, V., Ferguson, M., Gummer, D., Harris, E., Orelup, E., & Cox, A. (2006). The MSC50 wind and wave reanalysis. Proceedings of the 9th International Workshop on Wave Hindcasting and Forecasting, 25, 29.

Thijssen, J., Fuglem, M., Muggeridge, K., Morrison, T., & Spencer, P. (2015). Update on Probabilistic Assessment of Multi-year Sea Ice Loads on Vertical-faced Structures. OTC Arctic Technology Conference. OTC Arctic Technology Conference, Copenhagen, Denmark. https://doi.org/10.4043/25520-MS.